HHS Public Access

Author manuscript

Toxicol In Vitro. Author manuscript; available in PMC 2018 December 12.

Published in final edited form as:

Toxicol In Vitro. 2018 September ; 51: 40–49. doi:10.1016/j.tiv.2018.05.003.

Experimental challenges regarding the *in vitro* investigation of the nanoparticle-biocorona in disease states

Xue-Fu Sherleen Adamson[a], **Zhoumeng Lin**[b], **Ran Chen**[b], **Lisa Kobos**[a], and **Jonathan Shannahan**[a,*]

[a]School of Health Sciences, Purdue University, 550 Stadium Mall Dr, West Lafayette, IN 47907, United States

[b]Institute of Computational Comparative Medicine, Department of Anatomy and Physiology, College of Veterinary Medicine, Kansas State University, 1800 Denison Ave, Manhattan, KS 66506, United States

Abstract

Toxicological evaluation of nanoparticles (NPs) requires the utilization of *in vitro* techniques due to their number and diverse properties. Cell culture systems are often lacking in their ability to perform comparative toxicity assessment due to dosimetry issues and capacity to simulate *in vivo* environments. Upon encountering a physiological environment, NPs become coated with biomolecules forming a biocorona (BC), influencing function, biodistribution, and toxicity. Disease-induced alterations in the biological milieu can alter BC formation. This study evaluates the role of low-density lipoprotein (LDL) in altering macrophage responses to iron oxide (Fe_3O_4) NPs. BCs were formed by incubating Fe_3O_4 NPs in serum-free media, or 10% fetal bovine serum with or without LDL present. Following exposures to a normalized dose (25 μg/mL), macrophage association of Fe_3O_4 NPs with a LDL-BC was enhanced. TNF-α mRNA expression and protein levels were differentially induced due to BCs. Cell surface expression of SR-B1 was reduced following all Fe_3O_4 NPs exposures, while only NPs with an LDL-BC enhanced mitochondrial membrane potential. These findings suggest that elevations in LDL may contribute to distinct BC formation thereby influencing NP-cellular interactions and response. Further, our study highlights challenges that may arise during the *in vitro* evaluation of disease-related variations in the NP-BC.

Keywords

Dosimetry modeling; Low density lipoprotein; Macrophage; Tumor necrosis factor α; Scavenger receptors; Iron oxide

1. Introduction

Nanoparticles have the capacity to advance numerous fields of technology due to their unique physicochemical properties. Superparamagnetic iron oxide nanoparticles (Fe_3O_4

*Corresponding author. jshannah@purdue.edu (J. Shannahan).

Appendix A. Supplementary data

Supplementary data to this article can be found online at doi.org/10.1016/j.tiv.2018.05.003.

NPs) have been proposed for various biomedical applications such as their use as contrast agents for magnetic resonance imaging (MRI), carriers for target specific drug delivery and gene therapy, therapeutic agents for hyperthermia and anemia, and magnetic sensing probes for diagnostics (Neuberger et al., 2005; Tartaj et al., 2003, 2005; Babes 1999; Ghazanfari et al., 2016). These biomedical applications are due to Fe_3O_4 NP biocompatibility and relatively low toxicity, reduced sensitivity to oxidation, stability in magnetic response, as well as the ability to add surface modifications (Majewski and Thierry, 2007; Kim et al., 2006; Ghazanfari et al., 2016). The development of prospective NPs such as Fe_3O_4 has significantly increased the risk of human exposure to NPs (Dobrucki et al., 2015; Inturi et al., 2015; Ryan and Brayden, 2014). Upon the delivery *via* intravenous injection, NPs have direct contact with the blood circulation resulting in the potential for direct cardiovascular toxicity and subsequent systemic exposure to different organs and tissues. Understanding these interactions is necessary for the screening of early NP-induced toxicity. Thus, it is necessary to improve and develop *in vitro* approaches to accurately identify NP-induced toxicity prior to *in vivo* testing. This can be done by modifying *in vitro* exposure conditions to more accurately depict the *in vivo* environment, thereby, enhancing correlations between cell culture, animal, and human studies.

The blood circulation contains numerous proteins and lipids that can be adsorbed on the surface of NPs forming a biocorona (BC) (Lynch et al., 2007; Lundqvist et al., 2011; Monopoli et al., 2011, 2012; Vroman et al., 1980; Westmeier et al., 2016). The physicochemical properties of the NP (size, shape, surface charge, composition, and surface functional groups), the nature of the physiological environment (i.e., blood, interstitial fluid, and cytoplasm), and the exposure duration are essential factors governing the formation and composition of the NP-BC (Jedlovszky-Hajdú et al., 2012; Monopoli et al., 2011; Walkey and Chen, 2012; Walkey et al., 2014). The addition of BC results in alterations of NP properties such as size and interfacial composition, altered NP function, agglomeration, cellular uptake, transport, distribution, clearance, and toxicity (Beduneau et al., 2009; Clift et al., 2010; Lartigue et al., 2012; Maiorano et al., 2010; Rahman et al., 2013.). The NP-BC is a complex entity specific to each nanomaterial and the individual physiological environment. The surface of Fe_3O_4 NPs can be easily modified to target particular tissues, specifically for tumor targeting, however addition of the BC has been shown to interfere with NP targeting (Gupta and Gupta, 2005). The formation of BC on the surface of Fe_3O_4 NPs may influence their use as MRI contrast agents by interfering with their contrast abilities and altering biodistribution (Amiri et al., 2013; Kreuter, 2013). It remains unclear how the formation of BC on the surface of Fe_3O_4 NPs affects the functionality and toxicity of these NPs. To date, the majority of the investigations regarding the NP-BC has focused primarily on healthy scenarios conversely the majority of patients receiving NP-based treatments suffer from diseases that may modify the physiological environment and thereby alter the BC.

The American Heart Association has reported that over 33% of the adult population in the United States has high low-density lipoprotein (LDL) cholesterol levels (> 200mg/dl) (Mozaffarian et al., 2014). Subjects with high cholesterol levels have been shown to be susceptible to the toxicity resulting from NPs exposures compared to healthy individuals as the high LDL condition could modify the molecule profile of the blood circulation (Schwartz and Dockery, 1992; Schwartz and Morris, 1995). The formation of the BC is

primarily governed by the physiochemical properties of the NPs, time, and the physiological environment (Jedlovszky-Hajdú et al., 2012; Monopoli et al., 2011; Shannahan et al., 2013a, 2013b; Walkey and Chen, 2012; Walkey et al., 2014). In diseased physiological environments such as hyperlipidemia the blood contents of circulating macromolecules such as proteins, peptides, and lipids are modified, which could ultimately alter the composition of BC (Catalano et al., 1991; LaFramboise et al., 2012). The disease-modified BC may result in toxicological consequences different from those resulted from the BC formed under the healthy physiological environment. Previous research has demonstrated increased transcription of pro-inflammatory genes by endothelial cells when exposed to NPs with a hyperlipidemic BC compared to NPs with a normal BC (Shannahan et al., 2016). These disease-related discrepancies should be considered when using *in vitro* techniques to examine NP-induced toxicities as they highlight exacerbations in toxic responses that may occur in susceptible subpopulations.

In our current study, we evaluated the role of LDL in altering immune cell responses to NPs. Further we evaluated potential confounding factors that may influence the examination of disease-modified NP-BCs specifically related to altered cell culture dosimetry. BCs were formed by incubating Fe_3O_4 NPs in either 10% fetal bovine serum (FBS) with or without LDL present. Following the addition of the BCs, NP physiochemical properties were characterized. Macrophages were exposed to a normalized initial dose of 25 μg/mL of Fe_3O_4 NPs with or without BCs present. Lastly, we assessed the toxicological implications of these BCs on Fe_3O_4 NPs over a time-course by examining cytotoxicity, cell-NP association, deposition modeling, cell activation, and changes in the expression of scavenger receptor SR-B1 and mitochondrial membrane potential (MMP). Overall, by utilizing relevant exposure conditions that more accurately portray the *in vivo* environment in both healthy and diseased states, this study enhances our understanding of nanotoxicity, as well as, provides information necessary for the future *in vitro* assessment of NP-induced toxicity in diseased environments.

2. Materials and methods

2.1. Formation of Fe_3O_4 nanoparticle-biocorona

Spherical 20 nm Fe_3O_4 NPs suspended in water at a concentration of 20mg/mL were purchased from Nanocomposix (San Diego, CA) (Supplemental Fig. 1). LDL from human plasma was purchased from Lee Biosolutions (Maryland Heights, Mo) at a concentration of 4800 mg/dl. BCs were formed on Fe_3O_4 NPs as described in our recent publications (Shannahan et al., 2013a, b, 2015b, c, 2016). Briefly, Fe_3O_4 NPs were diluted in double deionized water (ddi H_2O) to the concentration of 1 mg/mL incubated for 2h at 4 °C in serum free medium (SFM), 10% fetal bovine serum (FBS), or 10% FBS + 200 mg/dL LDL while being mixed constantly. Specifically, 250 μL of Fe_3O_4 NPs (1 mg/mL) was combined with 750 μL SFM in a 1.5 mL tube referred to as the SFM-Fe_3O_4 NP group; 250 μL of Fe_3O_4 NPs (1 mg/mL) was combined with 650 μL SFM and 100 μL FBS in a 1.5 mL tube referred as the FBS-Fe_3O_4 NP group; and 250 μL of Fe_3O_4 NPs (1 mg/mL) was combined with 400 μL SFM, 100 μL FBS, and 250 μL LDL (final LDL concentration was 200mg/dL) in a 1.5 mL tube referred as the LDL-Fe_3O_4 NP group. Following the incubation, Fe_3O_4 NPs

were then pelleted *via* centrifugation at 3500 *g* for 10 min and washed with ddi H_2O. Fe_3O_4 NPs were resuspended in 500 μL ddi H_2O and pooled together within the same group. The Fe concentration of each group was quantified using atomic absorption spectrometry (AAS). Fe_3O_4 NPs from the above three incubation groups were then diluted in SFM to 20 μg Fe/mL approximately equal to 25 μg/mL Fe_3O_4 NPs for subsequent cell culture exposures. This concentration of Fe_3O_4 NPs was selected based on possible human exposures as well as previous *in vitro* examination of Fe_3O_4 NPs and other NPs (Shannahan et al., 2015b, 2015c, 2015d; Xia et al., 2013). Briefly, the concentration of Fe_3O_4 NPs was determined based on levels used for human MRI analysis using Fe_3O_4 NPs as a contrast agent, which typically range from 5 to 10 μg/mL blood volume, considering a male of 90 kg (Fukuda et al., 2006; Wang, 2011).

2.2. Characterization of Fe_3O_4 nanoparticle-biocorona

The hydrodynamic size and zeta potentials (ZetaSizer Nano, Malvern) of uncoated Fe_3O_4 NPs and Fe_3O_4 NPs with BCs were characterized in SFM with Fe_3O_4 NPs at a concentration of 50 μg/mL (n = 3/particle) (Table 1). Nanosight (Malvern) assessment of Fe_3O_4 NP counts determined 1.94 +/− 0.07 × 10^9 particles/μg.

2.3. In Vitro sedimentation, diffusion and dosimetry modeling

We applied the *In Vitro* Sedimentation, Diffusion and Dosimetry (ISDD) Model (Hinderliter et al., 2010) to predict the delivered doses based on our *in vitro* experimental settings. In brief, the primary particle size (approximately 25 nm), primary particle density (5.17 g/mL), exposure media volume (0.5 mL) for a 24-well cell culture plate (approximately 1.9 cm^2 growth area/well), media depth (2.63 mm or 0.00263 m), exposure concentrations of Fe_3O_4 NPs (6.25, 12.5, 25, or 50 μg/mL), and the hydrodynamic sizes of different NPs (listed in Table 1) were used in the model simulations. Default values of other parameters were used, including temperature of 310 K, media density of 1.0g/mL, and media viscosity of 0.00074 Pa s. The ISDD model is appropriate for our study as the model was developed for spherical particle exposures in monolayer cell culture systems using Fe_3O_4 NPs (Hinderliter et al., 2010).

2.4. Macrophage cell culture

RAW264.7 mouse macrophages were cultured in DMEM medium supplemented with 10% FBS and 100 U/mL penicillin-streptomycin. Macrophages were maintained in cell culture dishes under standard conditions at 37 °C and 5% CO_2. For the assessment of the BC and its role in cellular responses, all experiments were performed in SFM, as done in our previous experiments (Shannahan et al., 2015a, d, 2016). The removal of serum from medium allows for the evaluation of the intentionally formed BC without the addition of a secondary BC that would form within the cell culture system. The use of SFM limits the study of the BCs and cellular responses to short exposure time points.

2.5. Assessment of Fe_3O_4 NPs cytotoxicity

Macrophages were grown to 90% confluency in 24-well plates and were then exposed to 25 μg/mL Fe_3O_4 NPs with or without BCs for 1, 3, 6, 12, and 24 h in SFM. Changes in cell

viability were evaluated using the Thiazolyl Blue Tetrazolium Bromide (MTT) assay (Sigma Aldrich, St. Louis, MO) following manufacturer's instructions using a plate reader (Molecular Device). No overt cytotoxicity was identified across any of the time points therefore the concentration of 25 μg/mL Fe_3O_4 NPs was utilized for all subsequent experiments (Supplemental Fig. 2).

2.6. Transmission electron microscopy

(TEM) Analysis. Following exposure to 25 μg/mL Fe_3O_4 NPs with or without BCs for 24 h, macrophages were fixed with 2.5% glutaraldehyde in 0.1 M sodium cacodylate buffer, post-fixed in buffered 0.1% osmium tetroxide containing 0.8% potassium ferricyanide, and en bloc stained in 1% aqueous uranyl acetate. They were then dehydrated with a graded series of acetonitrile and embedded in Embed-812 resin. Thin sections (80 nm) were cut on a Reichert-Jung Ultracut E microtome and stained with 2% uranyl acetate and lead citrate. Thin sections were then mounted to 100 mesh Formvar/Carbon grids. TEM images were acquired using a Gatan Oriums side mount CCD camera on a FEI Tecnai T12 electron microscope equipped with a LaB6 source and operating at 80 kV.

2.7. Cellular association of Fe_3O_4 NPs

In order to determine BC-induced differential association of NPs with cells, association of Fe_3O_4 NPs with macrophages was quantified using AAS. Macrophages were grown to 90% confluency in 24-well plates and were exposed to 25 μg/mL Fe_3O_4 NPs with or without BCs for 3, 6, 12, and 24 h in SFM. Macrophages were harvested and then washed three times with PBS to remove extracellular excessive Fe_3O_4 NPs at the end of each time point exposure. The culture supernatant and PBS washes were also collected to quantify the amount of Fe_3O_4 NPs that remained in the medium that were not associated with cells. Analysis of the cell-associated and non-associated Fe_3O_4 NP fractions allowed for the determination of possible differential Fe_3O_4 NP plate binding resulting from the addition of the BC. Both cellular and medium Fe levels were determined using AAS after the measurement of protein quantity. All samples were digested with concentrated nitric acid (HNO_3) in an oven at 55 °C, overnight. A Varian Spectra AA-20 Plus GTA-96 flameless graphite furnace AAS was used to quantify Fe concentrations in macrophages and culture supernatant. Digested samples were diluted with 0.1% (v/v) HNO_3 for Fe measurement in order to keep the reading within the concentration range of the standard curve. The ranges of calibration standards were 0–10 μg/L for Fe and the detection limit for Fe was 0.9 ng/mL of the assay solution.

2.8. Fe_3O_4 NP-induced cellular inflammatory responses

Macrophages were grown to 90% confluency in 24-well plates and were exposed to 25 μg/mL Fe_3O_4 NPs with or without BCs for 1, 3, 6, 12, and 24 h in SFM. In addition, untreated macrophages cultured in SFM were used as the control group. Cells were harvested for total RNA isolation using TRIzol (Invitrogen). An aliquot of 1 μg RNA was reverse-transcribed into cDNA. BioRad iTaq Universal SYBR Green Supermix was used for quantitative real time RT-PCR (qPCR) analysis. The amplification was run in the CFX connect TM real-time PCR detection system (BioRad, CA). With an initial 3-min denaturation at 95 °C, the amplification program was followed by 40 cycles of 30 s

denaturation at 95 °C, 10s at 60 °C and 30 s extension at 72 °C. A dissociation curve was used to verify that the majority of fluoresce detected was attributed to the labeling of the specific PCR products, and also to verify the absence of primer dimers and sample contamination. Each real-time RT-PCR reaction was run in triplicate. Relative gene mRNA expression ratios between groups were calculated using the ΔΔCt formulation where Ct is the threshold cycle time value. The Ct values of interested genes were first normalized with that of beta actin *Actb* in the same sample to obtain the ΔΔCt values, and the relative ratios between control and treatment groups were calculated and expressed as relative gene expression by setting the control as 100%. The amplification efficiencies of target gene and the internal reference were examined by determining the variations of the Ct with a series of control template dilutions. The forward and reverse primers for the mouse *Tnf-α* and *Actb* genes were designed using Primer Express 3.0 software. Primers sequences for mouse *Tnf-α* used in this study were a forward primer 5′-CAG GCG GTG CCT ATG TCT C−3′ and a reverse primer 5′-CGA TCA CCC CGA AGT TCA GTA G −3′ (GenBank accession no. NM_013693). The mouse beta actin *Actb* used as an internal control had a forward primer 5′-ACG TTG ACA TCC GTA AAG A −3’ and a reverse primer 5′-GCC GGA CTC ATC GTA CTC C−3′ (GenBank accession no. NM_007393).

To confirm the qPCR results of *Tnf-α* mRNA expression, the intracellular and extracellular protein levels of TNF-α were quantified using ELISA assay. Macrophages were grown to 90% confluency in 24-well plates and were exposed to 25 μg/mL Fe_3O_4 NPs with or without BCs for 1, 3, 6, 12, 24, and 36 h in SFM. As the synthesis of protein occurs following mRNA transcription, a 36-h time point was included to assess the delayed protein levels of TNF-α. In addition, macrophages without NPs exposure were used as the control group. Macrophages and the culture supernatant were harvested to determine the produced intracellular level of TNF-α and the extracellular level of TNF-α released into culture supernatant, respectively, by ELISA (R & D systems, Minneapolis, MN) following the manufacturer's high sensitivity instructions. The ELISA kit uses a competitive binding method to assess the sample specific TNF-α. The intracellular TNF-α levels were normalized by protein quantity and expressed as pg/mg protein. The extracellular TNF-α levels were expressed as pg/mL in media.

2.9. Evaluation of cell surface SR-B1 receptor expression density following Fe_3O_4 NP exposure

Interactions between NPs and macrophages have been shown to occur through cell surface receptors such as scavenger receptors (Aldossari et al., 2015; Singh and Ramarao, 2012). Exposures can modify the surface expression of these receptors therefore we evaluated the expression of scavenger receptor-B1 (SR-B1) over the course of Fe_3O_4 NPs exposures with modified BCs. The surface expression of SR-B1 receptor in macrophages was determined following exposures to 25 μg/mL Fe_3O_4 NPs with or without BCs for 1, 3, 6, 12, and 24 h in SFM. Untreated macrophages in SFM at each time point were used as controls. At the end of exposures, cells were washed with PBS by spinning down (1000 rpm, 10 min), re-suspended, and fixed with 4% paraformaldehyde. After three washes with PBS, cells were then incubated with SR-B1 primary antibody (1:200) (Novus Biologicals, Littleton, CO) at room temperature for 1 h followed by three washes with PBS and the incubation of Alexa

Fluor 488 goat anti-rabbit IgG (H + L) secondary antibody (1500) (Life Technologies, Carlsbad, CA) at room temperature for 1 h. After three washes with PBS, cells were re-suspended in 300 μL PBS and analyzed using the flow cytometry (Accuri C6 Flow Cytometer, BD Biosciences, San Jose, CA). Alterations in macrophage SR-B1 expression were determined by calculating a fold change of individual sample fluorescence compared to the average fluorescence of the control group.

2.10. Assessment of mitochondrial membrane potential (MMP) following Fe_3O_4 NP exposure

Often alterations in mitochondrial endpoints are early events in cellular toxicity. To evaluate alterations in mitochondrial function, macrophages cultured in the 24-well plates were exposed to 25 μg/mL Fe_3O_4 NPs with or without BCs for 1, 3, 6, 12, and 24 h in SFM. Untreated macrophages in SFM at each time point were used as the control. At the end of exposures, the culture medium was removed and the cells were washed with PBS three times followed by the incubation with 10 μM Rhodamine 123 (Thermo Fisher Scientific, Grand Island, NY) in PBS at 37 °C for 15 min. Macrophages were pelleted and resuspended in 0.5 mL PBS after three washes with PBS. The cell suspension samples were then loaded into the black 96-well plate and read at 480 nm (Excitation)/520 nm (Emission) using a plate reader. A standard curve was created within the range of 0 to 10 μM Rhodamine 123 to determine the amount of Rhodamine 123. The BCA protein assay was used to determine the protein concentration of the cellular samples. The intracellular Rhodamine 123 levels were normalized by protein quantity and expressed as μM Rhodamine 123/mg protein.

2.11. Statistical analysis

All data are presented as mean ± SEM and consist of 3–6 experiments. Comparisons of the differences among the control and NPs exposed groups within the same time point were analyzed by one-way ANOVA with *post hoc* comparisons by Tukey test. All the statistical analyses were performed using GraphPad Prism 6 software (GraphPad, San Diego, CA). Statistical significance was determined when p value was found to be ≤0.05 between groups.

3. Results

3.1. Characterization of Fe_3O_4 NPs

Prior to BC formation, our TEM images presented in Supplemental Fig. 1 confirmed that the average size of the non-BC-coated Fe_3O_4 NPs was 24.7 ± 2.5 nm which was similar to our previous publication that TEM measurements found the diameter to be 25.0 ± 2.6 nm (Shannahan et al., 2016). Following formation of BCs, Fe_3O_4 NPs were assessed for alterations in hydrodynamic size and zeta potential compared to Fe_3O_4 NPs without BCs. Fe_3O_4 NPs incubated with H_2O or SFM underwent the same process as Fe_3O_4 NPs incubated with FBS or LDL to form the BC. Fe_3O_4 NPs with BCs (FBS or LDL) demonstrated significant increases in hydrodynamic size compared to Fe_3O_4 NPs incubated in H_2O or SFM ($p < 0.05$, Table 1). The evaluation of polydispersity index (PDI) revealed that Fe_3O_4 NPs with or without BC were in an intermediate, moderately polydisperse distribution type, while the formations of normal FBS-BC and LDL-BC showed significant increased PDI as compared with that of the SFM incubated Fe_3O_4 NPs suggesting increased

agglomeration ($p < 0.05$, Table 1). The addition of BCs was determined to reduce the zeta potential of Fe_3O_4 NPs, while the LDL-BC was found to result in the greatest reduction compared to the FBS-BC ($p < 0.05$, Table 1).

3.2. Evaluation of BC-induced alterations in cell viability

To determine possible differences in cytotoxicity due to the addition of the BCs, macrophages were exposed to the normalized 25 μg/mL Fe_3O_4 NPs with or without BCs for 1, 3, 6, 12, and 24 h in SFM and examined for differences in cell viability using MTT assay. Untreated macrophages in SFM were used as the control. No significant cytotoxicity was observed at the selected concentration of Fe_3O_4 NPs with or without BCs (25 μg/mL) for selected exposure time points (Supplemental Fig. 2).

3.3. In Vitro sedimentation, diffusion and dosimetry modeling

Based on the hydrodynamic sizes determined by dynamic light scattering (Table 1), cell culture deposition of Fe_3O_4 NPs with and without BCs was modeled. This model utilized typical cell culture parameters of a 24-well plate with well surface area of 1.9 cm^2, and 500 uL SFM volume with Fe_3O_4 NPs concentrations of 6.25, 12.5, 25, or 50 μg/mL. Examination of total deposited dose did not demonstrate differences in deposition trends due to Fe_3O_4 NP concentrations (Supplemental Fig. 3). Modeled deposition at early time points, typically evaluated for NP-BC cell interactions, of 1, 3, 6, and 12 h predicted a slight increase in deposition of Fe_3O_4 NPs without a BC compared to Fe_3O_4 NPs with BCs (Fig. 1A). At 48 h, it was predicted that the deposition of Fe_3O_4 NPs with a LDL-BC would begin to exceed those Fe_3O_4 NPs without a BC or with a FBS-BC (Fig. 1A). At 12 and 24 h, Fe_3O_4 NPs with a LDL-BC were found to increasingly associate with macrophages compared to those without BC or with a FBS-BC (Fig. 1B). Model predictions of later time points, that are typically not evaluated in NP-BC studies, demonstrated more pronounced differences in deposition with 100% of Fe_3O_4 NPs with LDL-BCs depositing earlier than Fe_3O_4 NPs without a BC and Fe_3O_4 NPs with a FBS-BC (Table 2).

3.4. Influence of BCs on the internalization of Fe_3O_4 NPs

To determine whether the addition of BCs influenced the cellular-association of Fe_3O_4 NPs, macrophages and culture supernatant were harvested following the exposure to 25 μg/mL Fe_3O_4 NPs with or without BCs for 1, 3, 6, 12, and 24 h in SFM to quantify the Fe contents using AAS. At the early exposure time points of 1, 3, and 6 h, Fe_3O_4 NPs without the BC associated with macrophages significantly more than the Fe_3O_4 NPs with BCs ($p < 0.05$, Fig. 1B). In addition, the cellular association of SFM-incubated Fe_3O_4 NPs reached plateau at 3h time point, while the cellular-association of Fe_3O_4 NPs with FBS- or LDL-BC showed a time-dependent increase from 1 to 12 h and reached a plateau at the 12 h time point (Fig. 1B). Consistently, as the cellular-association of Fe_3O_4 NPs increased and reached a plateau across the exposure time points, the Fe contents remained in the culture media reduced in a time-dependent manner until plateauing themselves (Fig. 1C). Since the Fe content of each exposure group was adjusted to the same amount at the beginning of the exposure, by subtracting the cellular-associated Fe and the remaining in the medium, the total plate-associated Fe content was calculated for each exposure group at each time point (Fig. 1D). Across all the exposure time points, the Fe_3O_4 NPs without BC and with FBS-BC appeared

to have more Fe adhered to the culture wells than that of Fe_3O_4 NPs with the LDL-BC ($p < 0.05$, Fig. 1D).

To confirm the association of Fe_3O_4 NPs with or without BCs with macrophages and to determine subcellular localization, macrophages were fixed and processed for TEM imaging following the exposure to 25 μg/mL Fe_3O_4 NPs with or without BCs for 24 h in SFM. Our TEM images confirmed the internalizations of Fe_3O_4 NPs with or without BCs (Fig. 2). The internalized NPs with or without BCs were encapsulated into membrane-bounded endosome-like vesicles distributed in the cytoplasm (Fig. 2). No Fe_3O_4 NPs were observed to distribute inside the organelles of mitochondria, endoplasmic reticulum, and nuclear (Fig. 2). In addition, as compared with the Fe_3O_4 NPs without BC, NPs with normal or hyperlipidemic BC appeared to be internalized more due to the presence of greater numbers and larger endosome-like vesicles in the cytoplasm (Fig. 2C, D, and E).

3.5. Variations in cellular inflammatory response due to differences in the Fe_3O_4 NP-BC

To determine whether the formation of BC induced the activation of macrophages, we measured the mRNA expression and protein levels of TNF-α in macrophages following the exposure to 25 μg/mL Fe_3O_4 NPs with or without BCs at 1, 3, 6, 12, and 24 h in SFM. All Fe_3O_4 NPs with or without BCs were found to induce mRNA expression of *Tnf-a* in macrophages across all the exposure time points except the exposures to Fe_3O_4 NPs with the FBS-BC or without BCs at the 12 h time point when these two exposures appeared to reduce the mRNA level of *Tnf-a* ($p < 0.05$, Fig. 3A). Across all of the evaluated exposure time points, macrophages exposed to the Fe_3O_4 NPs with the LDL-BC had the highest *Tnf-a* mRNA expression level, when compared with those of the control, SFM-Fe_3O_4 NPs, and FBS-Fe_3O_4 NPs groups ($p < 0.05$, Fig. 3A).

To confirm the mRNA expression findings of *Tnf-a,* we further quantified the intracellular and secreted protein levels of TNF- α of the macrophages using the ELISA assay. Due to likely delays in protein production as compared with mRNA expression, a 36-h time point was included with the other five exposure time points of 1, 3, 6, 12, and 24 h. During the early exposure time points of 1, 3, and 6 h, the intracellular TNF-α levels of all three Fe_3O_4 NPs-exposed groups showed a reduction over time but an elevation at the later exposure time points of 12, 24, and 36 h (Fig. 3B). In addition, the macrophages that were exposed to Fe_3O_4 NPs without a BC induced significantly higher productions of intracellular TNF-α protein than that of the control (all time points) and both groups exposed to Fe_3O_4 NPs with BCs (1, 3, and 12 h time points) ($p < 0.05$, Fig. 3B). The macrophages exposed to Fe_3O_4 NPs with a FBS-BC produced the highest level of TNF-α protein following 24 and 36 h exposures, when compared with the other groups ($p < 0.05$, Fig. 3B). At the end of 36 h exposure, the formation of LDL-BC resulted in a significantly higher level of intracellular macrophage TNF-α than those of the control and the group exposed to the Fe_3O_4 NPs without BC ($p < 0.05$, Fig. 3B). When the released TNF-α protein levels were evaluated in the culture supernatant, the macrophages from all three exposed groups appeared to secrete significantly higher amounts of TNF-α protein over time compared with that of the control ($p < 0.05$, Fig. 3C). Except for the 1 and 24 h time points, the highest level of TNF-α in the culture supernatant was released by the macrophages exposed to Fe_3O_4 NPs without a BC

(Fig. 3C). TNF-α levels were similarly elevated at 3, 6, and 12 h for Fe_3O_4 NPs with BCs, however, at 24 and 36 h TNF-α levels released in the media continued to increasing (Fig. 3C).

3.6. Fe_3O_4 NP exposures reduce cell surface receptor density of SR-B1

As a membrane receptor to facilitate the intake of foreign materials and lipoproteins, SR-B1 may play a role in the cellular uptake of NPs, especially for those NPs with a lipid-rich BC. To determine whether exposure to Fe_3O_4 NPs with or without BCs affected cell surface SR-B1 expression, macrophages were harvested following the exposure to 25 μg/mL Fe_3O_4 NPs with or without BCs for 1, 3, 6, 12, and 24 h for immunocytochemical staining and flow cytometry analysis. Our results revealed that all exposure groups across all time points except for the Fe_3O_4 NPs with a FBS-BC at 1 h significantly inhibited the surface expression of SR-B1 ($p < 0.05$, Fig. 4A, Representative FACs - Supplemental Fig. 4). All exposure groups began to trend towards controls at 12 and 24 h (Fig. 4A). In addition, following exposures for 1, 3, 6, and 24 h, macrophages exposed to Fe_3O_4 NPs with a LDL-BC showed significant lower expression of SR-B1 than those exposed to FBS-coated Fe_3O_4 NPs (Fig. 4A).

3.7. Fe_3O_4 NP-BC induces alterations in MMP

Upon entering macrophages, Fe_3O_4 NPs may directly or indirectly interfere with mitochondrial function. Disruption of MMP is considered an early toxicity event leading to oxidative stress and possibly apoptosis. To determine whether the Fe_3O_4 NPs with normal or hyperlipidemia BC induced mitochondrial dysfunction, macrophages exposed to 25 μg/mL of Fe_3O_4 NPs with or without BCs for 1, 3, 6, 12, and 24 h were stained with Rhodamine 123, a tracer dye that can accumulate in the polarized membranes within the mitochondria. A higher accumulation of Rhodamine 123 suggests an increase in the mitochondria membrane polarization. After being normalized to protein content, macrophages exposed to the Fe_3O_4 NPs with LDL-BC appeared to induce markedly higher accumulations of Rhodamine 123 at the early 1 h time point and the later 12 and 24 h time points ($p < 0.05$, Fig. 4B). In addition, across all the exposure time points, the exposures of the Fe_3O_4 NPs without BC and with the normal FBS-BC only showed increased Rhodamine 123 accumulation at 24 h exposure time point ($p < 0.05$, Fig. 4B).

4. Discussion

The adsorption of proteins on the surface of NPs can modify their chemical and physical properties, such as size and surface charge, which can influence cellular uptake and biodistribution leading to modifications of their therapeutic applications and toxicity. Studies have demonstrated that underlying physiological disease condition such as hyperlipidemia can modify BC formation and cell responses (Shannahan et al., 2015b, 2016). In the current *in vitro* study the role of the specific hyperlipidemic component LDL was evaluated due to the prevalence of individuals in our population existing with elevated circulating levels. Our data demonstrate that: (1) the formation of BC markedly increases the hydrodynamic size but reduces the Zeta potential of Fe_3O_4 NPs; (2) the addition of LDL into the BC enhances deposition, uptake and internalization of Fe_3O_4 NPs; (3) both mRNA and protein

expressions of TNF-α are differentially induced in the macrophages exposed to Fe_3O_4 NPs with variations in the BC; (4) the cell surface expression of SR-B1 is inhibited following all Fe_3O_4 NPs exposures; and (5) the addition of LDL-BC to the Fe_3O_4 NPs appears to increase MMP. Overall, these findings suggest that elevations in LDL may contribute to distinct BC formation on the surface of NPs thereby influencing the NP-cellular interactions, altering NP kinetics, cellular uptake and inflammatory response. Further, our study also highlights specific challenges such as simulating *in vivo* differential susceptibilities between healthy subjects and subjects under disease states to NPs that may arise during the *in vitro* evaluation of disease-related variations in the NP-BC formation.

When quantifying the uptake amount of Fe_3O_4 NPs, our AAS results distinctly revealed that the NPs without BC were quickly taken up by the macrophages and reached a plateau within 3 h, while the uptake of the NPs with BC appeared in a time-dependent manner and reached the plateau at approximately 12 h (Fig. 1B). This outcome was similar to our ISDD model-predicted result that NPs without BC were deposited slightly more at the earlier time points (Fig. 1A). Specifically, at the very early time point of 1 h, the depositions of Fe_3O_4 NPs with FBS- and LDL-BC were the same but more Fe_3O_4 NPs without BC were found to deposit in the 24-well plate (Fig. 1A). While at the later time points of 12, 24, and 48 h, the deposition of LDL-coated Fe_3O_4 NPs was higher than FBS-BC Fe_3O_4 NPs (Fig. 1A). This predicted result is also consistent with the observation that the Fe_3O_4 NPs with LDL-BC were taken up more by macrophages than those with FBS-BC (Fig. 1B). Interestingly, the highest uptake level of Fe_3O_4 NPs appeared to be the NPs with the LDL-BC at the later time points of 12 and 24 h (Fig. 1B). Since the plateau for Fe_3O_4 NPs with a LDL-BC was higher it appears to indicate preferential internalization of Fe_3O_4 NPs coated with the LDL-BC by macrophages and interactions between the two compared to other exposure groups. This uptake preference may be due to increased interactions with receptors such as scavenger class receptors that are expressed on macrophages, which can recognize a number of ligands including oxidized-lipoproteins, pathogens, and negatively charged foreign particles (Prabhudas et al., 2014). Further, Fe_3O_4 NPs with the LDL-BC were found to have a significantly lower adherence to the culture plate and the binding of NPs to the plate seemed to be immediate and not alter over time (Fig. 1D) thereby, it might lead to a higher delivery dose for the NPs with LDL-BC. In addition, when validating the internalization of Fe_3O_4 NPs in macrophages, more and larger membrane-encapsulated endosome-like NPs vesicles were observed in macrophages exposed to Fe_3O_4 NPs with normal or hyperlipidemic BCs than those exposed to NPs without BC (Fig. 2). This phenomenon may assist in explaining the increased uptake of Fe_3O_4 NPs by macrophages with the presence of BCs.

The SR-B1 receptor belongs to the class B scavenger receptors and is abundantly expressed in macrophages, platelets, hepatocytes, endothelial and epithelial cells (Dieudonne et al., 2012; Kzhyshkowska et al., 2012; Rigotti et al., 1997; Uittenbogaard et al., 2000). SR-B1 receptor has been shown to be involved with cholesterol metabolism (Rigotti et al., 1997, 2003) and be a potential target for a variety nanotherapeutics and diagnostic applications (Mooberry et al., 2010; Shahzad et al., 2011; Zheng et al., 2013). Our previous studies have demonstrated the inhibition of SR-B1 significantly reduced the uptake of AgNPs in macrophages, endothelial and epithelial cells, as well as the induced protein levels of the inflammatory cytokine osteopontin (Aldossari et al., 2015; Shannahan and Brown, 2014,

Shannahan et al., 2015b), suggesting that the uptake of NPs and NPs-induced inflammatory responses might be mediated *via* SR-B1. Our current results clearly showed that the cell surface expression of SR-B1 was significantly inhibited by all three exposures along all evaluated time points (Fig. 4A), indicating that SR-B1 receptors may serve as the target binding site of NPs to mediate the cellular uptake. As a cell surface molecule likely to mediate endosomal and liposomal trafficking, SR-B1 might be internalized due to its affinity with lipid BC-coated NPs resulting in decreased surface expression (Yang et al., 2013; Sakai-Kato et al., 2017). Therefore, the more binding of NPs, likely leads to less expression of SR-B1 on the macrophage surface. Although SR-B1 was downregulated during the exposure, we observed a time-dependent restoration in SR-B1 expression during later time points, thereby, the macrophage may be recycling SR-B1 receptors to the surface or increased receptor synthesis and presentation. Overall, these findings suggest a role for SR-B1 in mediating the macrophage response to NPs, which will likely influence the cellular uptake, clearance, activity, and immune responses of NPs. It is also likely that the macrophage's response to a subsequent pathogen challenge following NP-induced downregulation of SR-B1 may be hindered or modified. In our current study, we only evaluated a single cell surface receptor but it is likely that other scavenger receptors may have been modified as well that could alter macrophage responses.

Our AAS results revealed that macrophages associated over 60% of the total dosed Fe_3O_4 NPs at the plateau for all groups, with the highest intake occurred in the exposure to Fe_3O_4 NPs with the LDL-enriched BC (about 80% of the total dosed Fe_3O_4 NPs, Fig. 1B). In addition, the difference in plate binding was shown to be much less than that taken up by macrophages suggesting that this differential uptake may not be due to availability differences related to plate binding (Fig. 1D). The interactions with Fe_3O_4 NPs, likely resulted in activation of the macrophage inflammatory response by inducing the mRNA and protein levels of TNF-α (Fig. 3A to C). Consistent with the AAS results, across all the selected exposure time points, the highest mRNA expression of *Tnf-α* was induced within the macrophages exposed to Fe_3O_4 NPs with the LDL-enriched BC (Fig. 3A). These findings suggest that there may be a link between the cellular uptake and activation/inflammatory responses in macrophages. However, the transcriptional mRNA changes did not correspond with the protein levels produced within the macrophages and secreted into the culture media, more specifically, the LDL-BC did not produce or secrete the highest TNF-α protein (Fig. 3B and C). This discrepancy between mRNA and protein levels is possibly due to 1) differential binding of produced TNF-α protein to NPs due to the addition of the BCs, 2) delay or inhibited translation from mRNA to protein, and/or 3) modifications in protein degradation. In addition, the secreted TNF-α protein in the media increased in a time-dependent manner, while the intracellular TNF-α level appeared a “U” shaped change over time. It is worth noting that controls demonstrated a reduced intracellular TNF-α levels likely due to having their media changed when exposures occurred. Further, to maintain a basal homeostasis of TNF-α between the intracellular and extracellular compartments, the low concentration of TNF-α in the culture media at early time points may trigger the production and secretion of TNF-α by the cells. With the continuous secretion as the exposure time increased, more TNF-α was released into the media building up to a higher level. However, longer exposure resulted in the increased production of TNF-α, which

contributed to the significant elevations of intracellular and extracellular TNF-α level. In our previous study, we found that the addition of high-density lipoprotein-enriched BC on the surface of silver NPs (AgNPs) decreased the internalization by rat lung epithelial cells but exacerbated the inflammatory response, as compared with the AgNPs without BC (Shannahan et al., 2015b). Taken together, the physicochemical properties and the characteristics of the BC, which influence the cellular association of NPs, are complex and are modulated by a variety of factors, thereby, they may lead to differential bioreactions.

To further explore the underlying mechanisms by which Fe_3O_4 NPs exposure induce potential toxicological consequences, we used the Rhodamine 123 to evaluate the mitochondria as a target organelle whose function may be modified due to the addition of the BC on NPs. Rhodamine is a tracer dye used to evaluate the membrane polarization of the mitochondria, exposure of live cells to a low dose of Rhodamine 123 results in selective accumulation of this dye in mitochondria (Chen, 1988; Darzynkiewicz et al., 1982; Huang et al., 2007). MMP plays a critical role in maintaining the normal function of the respiratory chain to generate ATP. A significant loss or induction of MMP can result in ATP depletion leading to the generation of reactive oxygen species (ROS) and ultimately apoptosis. In current study, the addition of LDL-enriched BC was found to significantly induce the cellular accumulation of Rhodamine 123 at the early 1 h and later 12 and 24 h time points, while the Fe_3O_4 NPs without BC or with normal FBS-BC increased the accumulation of Rhodamine 123 only at the last time point (Fig. 4B). Further, as compared with the early time points, there was a significant jump in the accumulation of Rhodamine 123 at 24 h time point (Fig. 4B). These results indicate that the Fe_3O_4 NPs exposure induces a hyperpolarization of MMP, which is more profound following the exposure to the NPs with LDL-enriched BC. This disruption of MMP is considered as an early even of ROS-mediated apoptosis (Banki et al., 1999; Gottlieb et al., 2000; Li et al., 1999). The LDL-BC preferential hyperpolarization of MMP suggests that the LDL-specific proteins bound on the surface of the NPs may be the key players that trigger the mitochondrial malfunction in macrophages through indirect reactions since our TEM evidence didn't show direct interaction of Fe_3O_4 NPs and mitochondria (Fig. 2), which requires further investigation. Further, as the Fe_3O_4 NPs with LDL-BC were preferentially taken up by the macrophages in more and larger membrane encapsulated vesicles (Fig. 2C and F), whether these NPs accumulate on site within the mitochondria remain elucidated. In addition, future studies on mitochondrial bioenergetics are needed to evaluate BC-induced alterations in mitochondrial function as our data suggests that it may be differential affected by LDL-rich BCs. Thereby, when assessing the toxicity of Fe_3O_4 NPs in human beings, the mitochondrial function could be an important parameter to be evaluated in the population with high LDL.

The major challenges our study evaluated are related to dosimetry differences in the *in vitro* evaluation of the NP-BC. In the current study the exposure dose of all three Fe_3O_4 NPs with or without BC was accurately normalized to 25 μg/mL after the incubation with SFM, FBS or LDL-enriched media using the AAS, which insured that the initial exposure amount for Fe was comparable among different BC groups. Due to the different sizes and surface charges of the Fe_3O_4 NPs after formation of the BCs, the preparation cycle of centrifuge, rinse, and resuspension, loss of NPs can occur. This loss of NPs during processing can cause inequivalent final concentrations of NPs due to the BC. Without normalizing the final doses

of Fe_3O_4 NPs, cells will receive unknown differential amounts of NPs and yield cellular toxicity data that is not comparable. Therefore, this normalization step is essential and adds to the accuracy, consistency, and confidence to the study design and result interpretation. Our current study also demonstrated that addition of distinct BCs resulted in differential interactions with typical cell culture plates causing possible alterations in dosimetry. Specifically, we found that addition of LDL to the Fe_3O_4 NP-BC decreased plate binding making more Fe_3O_4 NPs available for cellular interactions. Lastly, our study utilized the ISDD model to determine BC-induced differences in deposition within cell culture systems. It was determined that at early time points of 24 h or less there were relatively minor differences in modeled deposition between the three studied groups. It was predicted that at later time points the differences in deposition would be more pronounced, with the LDL-BC-coated Fe_3O_4 NPs having the highest deposition. Due to the removal of serum from the media that is typically done in *in vitro* studies to evaluate the BC studies are limited to early time points. Therefore, alterations in deposition of NPs due to addition of the BC likely do not greatly impact *in vitro* studies evaluating cellular responses.

Although the current study attempted to depict the toxicological consequences induced by the BC formation by studying various effects of NPs-BC on cytotoxicity, cellular uptake, inflammatory responses, SR-B1 expression and MMP, in-depth studies are necessary to: (1) further determine the subcellular distribution overtime, Fe dissociation, metabolism and clearance, ROS generation, mitochondrial function after NPs exposure, (2) characterize alterations in protein profiles of BCs due to the presence of LDL, (3) identify the specific BC proteins that contribute to the differential toxicological consequences, and (4) explore the underlying mechanisms and pathways of toxicity related to NP physicochemical properties and the BC. Based on our findings, we recommend that *in vitro* studies attempt to incorporate disease-related physiological alterations such as distinct BC formation in order to more accurately predict the *in vivo* environment thereby improving the translatability of *in vitro* studies. Further, we suggest that experiments analyze a variety of time points when investigating the BC since cellular responses differ over time. Lastly, studies need to be designed to accommodate for BC-induced modifications in dosimetry that may occur.

Supplementary Material

Refer to Web version on PubMed Central for supplementary material.

Acknowledgement

Electron microscopy was performed with the help of staff in the Life Science Microscopy Facility at Purdue University. The authors would like to acknowledge Dr. Justin G. Teeguarden at Pacific Northwest National Laboratory, Richland, WA for providing the *in vitro* sedimentation, diffusion and dosimetry (ISDD) model.

Funding

This work was supported by the National Institute of Environmental Health SciencesR00 ES 024392 (JS) and the K-State Mentoring Fellowship (ZL).

References

Aldossari AA, Shannahan JH, Podila R Brown JM, 2015 Influence of physicochemical properties of silver nanoparticle on mast cell activation and degranulation. Toxicol. in Vitro 29, 195–203. [PubMed: 25458489]

Amiri H, Bordonali L, Lascialfari A, Wan S, Monopoli MP, Lynch I, Laurent S, Mahmoudi M, 2013 Protein corona affects the relaxivity and MRI contrast efficiency of magnetic nanoparticles. Nano 5 (18), 8656–8665.

Babes L, Denizot B, Tanguy G, Le Jeune JJ, Jallet P, 1999 Synthesis of iron oxide nanoparticles used as MRI contrast agents: A parametric study. J Colloid Interf Sci 212, 474–482.

Banki K, Hutter E, Gonchoroff N, Perl A, 1999 Elevation of mitochondrial transmembrane potential and reactive oxygen intermediate levels are early events and occur independently from activation of caspases in Fas signaling. J. Immunol 162, 1466–1479. [PubMed: 9973403]

Beduneau A, Ma Z, Crotepas CB, Kabanov A, Rabinow BE, Gong N, Mosley RL, Dou H, Boska MD, Gendelman HE, 2009 Facilitated monocyte-macrophage uptake and tissue distribution of superparmagnetic iron-oxide nanoparticles. PLoS One 4 (2), e4343. [PubMed: 19183814]

Catalano M, Aronica A, Carzaniga G, Seregni R, Libretti A, 1991 Serum lipids and apolipoproteins in patients with essential hypertension. Atherosclerosis 87 (1), 17–22. [PubMed: 1872922]

Chen LB, 1988 Mitochondrial membrane potential in living cells. Annu. Rev. Cell Biol 4, 155–181. [PubMed: 3058159]

Clift MJ, Bhattacharjee S, Brown DM, Stone V, 2010 The effects of serum on the toxicity of manufactured nanoparticles. Toxicol. Lett 198 (3), 358–365. [PubMed: 20705123]

Darzynkiewicz Z, Traganos F, Staiano-Coico L, Kapuscinski J, Melamed MR, 1982 Interaction of rhodamine 123 with living cells studies by flow cytometry. Cancer Res. 42 (3), 799–806. [PubMed: 7059978]

Dieudonne A, Torres D, Blanchard S, Taront S, Jeannin P, Delneste Y, Pichavant M, Trottein F, Gosset P, 2012 Scavenger receptors in human airway epithelial cells: role in response to double-stranded RNA. PLoS One 7 (8), e41952. [PubMed: 22879901]

Dobrucki LW, Pan D, Smith AM, 2015 Multiscale imaging of nanoparticle drug delivery. Curr. Drug Targets 16 (6), 560–570. [PubMed: 25642717]

Fukuda Y, Ando K, Ishikura R, Kotoura N, Tsuda N, Kato N, Yoshiya S, Nakao N, 2006 Superparamagnetic iron oxide (SPIO) MRI contrast agent for bone marrow imaging: differentiating bone metastasis and osteomyelitis. Magn. Reson. Med. Sci 5 (4), 191–196. [PubMed: 17332709]

Ghazanfari MR, Kashefi M, Shams SF, Jaafari MR, 2016 Perspective of Fe_3O_4 nanoparticles role in biomedical applications. Biochem. Res. Int. 2016, 7840161. [PubMed: 27293893]

Gottlieb E, Vander Heiden MG, Thompson CG, 2000 Bcl-XL prevents the initial decrease in mitochondrial membrane potential and subsequent reactive oxygen species production during tumor necrosis factor α-induced apoptosis. Mol. Cell. Biol 20, 5680–5689. [PubMed: 10891504]

Gupta AK, Gupta M, 2005 Synthesis and surface engineering of iron oxide nanoparticles for biomedical applications. Biomaterials 26 (18), 3995–4021. [PubMed: 15626447]

Hinderliter PM, Minard KR, Orr G, Chrisler WB, Thrall BD, Pounds JG, Teeguarden JG, 2010 ISDD: a computational model of particle sedimentation, diffusion and target cell dosimetry for in vitro toxicity studies. Part. Fibre Toxicol 7, 36. [PubMed: 21118529]

Huang M, Camara AK, Stowe DF, Qi F, Beard DA, 2007 Mitochondrial inner membrane electrophysiology assessed by rhodamine-123 transport and fluorescence. Ann. Biomed. Eng 35 (7), 1276–1285. [PubMed: 17372838]

Inturi S, Wang G, Chen F, Banda NK, Holers VM, Wu L, Moghimi SM, Simberg D, 2015 Modulatory role of surface coating of superparamagnetic iron oxide nanoworms in complement opsonization and leukocyte uptake. ACS Nano 9 (11), 10758–10768. [PubMed: 26488074]

Jedlovszky-Hajdú A, Bombelli FB, Monopoli MP, Tombacz E, Dawson KA, 2012 Surface coatings shape the protein corona of SPIONs with relevance to their application in vivo. Langmuir 28 (42), 14983–14991. [PubMed: 23002920]

Kim JS, Yoon TJ, Yu KN, Kim BG, Park SJ, Kim HW, Lee KH, Park SB, Lee JK, Cho MH, 2006 Toxicity and tissue distribution of magnetic nanoparticles in mice. Toxicol. Sci 89 (1), 338–347. [PubMed: 16237191]

Kreuter J, 2013 Mechanism of polymeric nanoparticle-based drug transport across the blood-brain barrier (BBB). J. Microencapsul 30, 49–54. [PubMed: 22676632]

Kzhyshkowska J, Neyen C,, Gordon S, 2012 Role of macrophage scavenger receptors in atherosclerosis. Immunobiology 217, 492–502. [PubMed: 22437077]

LaFramboise WA, Dhir R, Kelly LA, Petrosko P, Krill-Burger JM, Sciulli CM, Lyons-Weiler MA, Chandran UR, Lomakin A, Masterson RV, Marroquin OC, Mulukutla SR, McNamara DM, 2012 Serum protein profiles predict coronary artery disease I nsympotomatic patients referred for coronary angiography. BMC Med 10, 157. [PubMed: 23216991]

Lartigue L, Wilhelm C, Servais J, Factor C, Dencausse A, Bacri JC, Luciani N,, Gazeau F, 2012 Nanomagnetic sensing of blood plasma protein interactions with iron oxide nanoparticles: impact on macrophage uptake. ACS Nano 6 (3), 2665–2678. [PubMed: 22324868]

Li P, Dietz R, von Harsdorf R, 1999 p53 regulates mitochondrial membrane potential through reactive oxygen species and induces cytochrome c-independent apoptosis blocked by bcl-2. EMBO J. 18, 6027–6036. [PubMed: 10545114]

Lundqvist M, Stigler J, Cedervall T, Berggad T, Flanagan MB, Lynch I, Elia G, Dawson K, 2011 The evolution of the protein corona around nanoparticles: a test study. ACS Nano 5 (9), 7503–7509. [PubMed: 21861491]

Lynch I, Cedervall T, Lundgvist M, Cabaleiro-Lago C, Linse S, Dawson KA, 2007 The nanoparticle-protein complex as a biological entity; a complex fluids and surface science challenge for the 21st century. Adv. Colloid Interf. Sci 134–135, 157–174.

Maiorano G, Sabella S, Sorce B, Brunetti V, Malvindi MA, Cingolani R, Pompa PP, 2010 Effects of cell culture media on the dynamic formation of protein-nanoparticl complexes and influence on the cellular response. ACS Nano 4 (12), 7481–7491. [PubMed: 21082814]

Majewski P, Thierry B, 2007 Functionalized magnetite nanoparticles – synthesis, properties, and bio-applications. Crit. Rev. Solid State Mater. Sci 32 (3–4), 203–215.

Monopoli MP, Walczyk D, Campbell A, Elia G, Lynch I, Bombelli FB, Dawson KA, 2011 Physical-chemical aspects of protein corona: relevance to in vitro and in vivo biological impacts of nanoparticles. J. Am. Chem. Soc 133, 2525–2534. [PubMed: 21288025]

Monopoli MP, Aberg C, Salvati A, Dawson KA, 2012 Biomolecular coronas provide the biological identity of nanosized materials. Nat. Nanotechnol 7 (12), 779–786. [PubMed: 23212421]

Mooberry LK, Nair M, Paranjape S, McConathy WJ, Lacko AG, 2010 Receptor mediated uptake of paclitaxel from a synthetic high density lipoprotein nanocarrier. J. Drug Target 18, 53–58. [PubMed: 19637935]

Mozaffarian D, Benjamin EJ, Go AS, Arnett DK, Blaha MJ, Cushman M, et al., 2014 Heart disease and stroke statistics – 2015 update: a report from the American Heart Association. Circulation e80.

Neuberger T, Schüpf B, Hofmann H, Hofmann M, Rechenberg von B, 2005 Superparamagnetic nanoparticles for biomedical applictions: possibilities and limitations of a new drug delivery system. J. Magn. Magn. Mater. 293 (1), 483–496.

Prabhudas M, Bowdish D, Drickamer K, Febbraio M, Herz J, Kbzik L, Krieger M, Loike J, Means TK, Moestrup SK, Post S, Sawamura T, Silverstein S, Wang XY, El Khoury J, 2014 Standardizing scavenger receptor nomenclature. J. Immunol 192 (5), 1997–2006. [PubMed: 24563502]

Rahman M, Laurent S, Tawil N, Yahia L, Mahmoudi M, 2013 Protein-Nanoparticle Interactions. Springer Series in Biophysics, vol. 15 Springer, Berlin Heidelberg, Berlin, Heidelberg (ISBN 978-3-642-37554-5).

Rigotti A, Trigatti BL, Penman M, Rayburn H, Herz J, Krieger M, 1997 A targeted mutation in the murine gene encoding the high density lipoprotein (HDL) receptor scavenger receptor class B type 1 reveals its key role in HDL metabolism. Proc. Natl. Acad. Sci. U. S. A 94, 12610–12615. [PubMed: 9356497]

Rigotti A, Miettinen HE, Krieger M, 2003 The role of the high-density lipoprotein receptor SR-B1 in the lipid metabolism of endocrine and other tissues. Endocr. Rev 24, 358–387.

Ryan SM, Brayden DJ, 2014 Progress in the delivery of nanoparticle constructs: towards clinical translation. Curr. Opin. Pharmacol 18, 120–128. [PubMed: 25450066]

Sakai-Kato K, Sakurai M, Takechi-Haraya Y, Nanjo K, Goda Y, 2017 Involvment of scavenger receptor class B type 1 and low-density lipoprotein receptor in the internalization of liposomes into HepG2 cells. Biochim. Biophys. Acta 1859 (11), 2253–2258.

Schwartz J, Dockery DW, 1992 Increased mortality in Philadelphia associated with daily air pollution concentrations. Am. Rev. Respir. Dis 145 (3), 600–604. [PubMed: 1546841]

Schwartz J, Morris R, 1995 Air pollution and hospital admissions for cardiovascular disease in Detroit, Michigan. Am. J. Epidemiol 142 (1), 23–35. [PubMed: 7785670]

Shahzad MM, Mangala LS, Han HD, Lu C, Bottsford-Miller J, Nishimura M, Mora EM, Lee JW, Stone RL, Pecot CV, Thanapprapasr D, Roh JW, Gaur P, Nair MP, Park YY, Sabnis N, Deavers MT, Lee JS, Ellis LM, Lopez-Berestein G, McConathy WJ, Prokai L, Lacko AG, Sood AK, 2011 Targeted delivery of small interfering RNA using reconstituted high-density lipoprotein nanoparticles. Neoplasia 13 (4), 309–319. [PubMed: 21472135]

Shannahan JH, Brown JM, 2014 Engineered nanomaterial exposure and the risk of allergic disease. Curr. Opin. Allergy Clin. Immunol 14, 95–99. [PubMed: 24378479]

Shannahan JH, Brown JM, Chen R, Ke PC, Lai X, Mitra S, Witzmann FA, 2013a Comparison of nanotube-protein corona composition in cell culture media. Small 9 (12), 2171–2181. [PubMed: 23322550]

Shannahan JH, Lai X, Ke PC, Podila R, Brown JM, Witzmann FA, 2013b Silver nanoparticle protein corona composition in cell culture media. PLoS One 8 (9), e74001. [PubMed: 24040142]

Shannahan JH, Bai W, Brown JM, 2015a Implications of scavenger receptors in the safe development of nanotherapeutics. Receptors Clin. Investig 2 (3), e811.

Shannahan JH, Podila R, Aldossari AA, Emerson H, Powell BA, Ke PC, Rao AM, Brown JM, 2015b Formation of a protein corona on silver nanoparticles mediates cellular toxicity via scavenger receptors. Toxicol. Sci 143 (1), 136–146. [PubMed: 25326241]

Shannahan JH, Podila R, Brown JM, 2015c A hyerspectral and toxicological analysis of protein corona impact on silver nanoparticle properties, intracellular modifications and macrophage activation. Int. J. Nanomedicine 10, 6509–6521. [PubMed: 26508856]

Shannahan JH, Sowrirajan H, Persaud I, Podila R, Brown JM, 2015d Impact of silver and iron nanoparticle exposure on cholesterol uptake by macrophages. J. Nanomater 2015, 127235 http://dx.doi.org/10.1155/2015/127235.12 pages. [PubMed: 29606957]

Shannahan JH, Fritz KS, Raghavendra AJ, Podila R, Brown JM, 2016 Disease-induced disparities in formation of nanoparticle-biocorona and the toxicological consequences. Toxicol. Sci 152 (2), 406–416. [PubMed: 27255384]

Singh RP, Ramarao P, 2012 Cellular uptake, intracellular trafficking and cytotoxicity of silver nanoparticles. Toxcol. Lett 213 (2), 249–259.

Tartaj P, Morales MP, Veintemillas-Verdaguer S, González-Carreno T, Serna CJ, 2003 The preparation of magnetic nanoparticles for applications in biomedicine. J. Phys. D 36 (13), R182–R197.

Tartaj P, Morales MP, González-Carreno T, Veintemillas-Verdaguer S, Serna CJ, 2005 Advances in magnetic nanoparticles for biotechnology applications. J. Magn. Magn. Mater 290–291 (part 1), 28–34.

Uittenbogaard A, Shaul PW, Yuhanna IS, Blair A, Smart EJ, 2000 High density lipoprotein prevents oxidized low density lipoprotein-induced inhibition of endothelial nitric-oxide synthase localization and activation in caveolae. J. Biol. Chem. 275, 11278–11283. [PubMed: 10753938]

Vroman L, Adams AL, Fischer GC, Munoz PC, 1980 Interaction of high molecular-weight kininogen, factor-Xii, and fibrinogen in plasma at interfaces. Blood 55, 156–159. [PubMed: 7350935]

Walkey CD, Chen WC, 2012 Understanding and controlling the interaction of nanomaterials with proteins in a physiological environment. Chem. Soc. Rev 41 (7), 2780–2799. [PubMed: 22086677]

Walkey CD, Olsen JB, Song F, Liu R, Guo H, Olsen DW, Cohen Y, Emili A, Chan WC, 2014 Protein corona fingerprinting predicts the cellular interaction of gold and silver nanoparticles. ACS Nano 8 (3), 2439–2455. [PubMed: 24517450]

Wang YX, 2011 Superparamagnetic iron oxide based MRI contrast agents: current status of clinical application. Quant. Imaging Med. Surg 1 (1), 35–40. [PubMed: 23256052]

Westmeier D, Stauber RH, Docter D, 2016 The concept of bio-corona in modulating the toxicity of engineered nanomaterials (ENM). Toxicol. Appl. Pharmacol 299, 53–57. [PubMed: 26592323]

Xia T, Hamilton RF, Bonner JC, Crandall ED, Elder A, Fazlollahi F, Girtsman TA, Kim K, Mitra S, Ntim SA, Orr G, Tagmount M, Taylor AJ, Telesca D, Tolic A, Vulpe CD, Walker AJ, Wang X, Witzmann FA, Wu N, Xie Y, Zink JI, Nel A, Holian A, 2013 Interlaboratory evaluation of in vitro cytotoxicity and inflammatory responses to engineered nanomaterials: the NIEHS Nano GO Consortium. Environ. Health Perspect 121 (6), 683–690. [PubMed: 23649538]

Yang XP, Amar MJ, Vasisman B, Bocharov AV, Vishnyakova TG, Freeman LA, Kurlander RJ, Patterson AP, Becker LC, Remaley AT, 2013 Scavenger receptor-B1 is a receptor for lipoprotein (a). J. Lipid Res. 54 (9), 2450–2457. [PubMed: 23812625]

Zheng Y, Liu Y, Jin H, Pan S, Qian Y, Huang C, Zeng Y, Luo Q, Zeng M, Zhang Z, 2013 Scavenger receptor B1 is a potential biomarker of human nasopharyngeal carcinoma and its growth is inhibited by HDL-mimetic nanoparticles. Theranostics 3 (7), 477–486. [PubMed: 23843895]

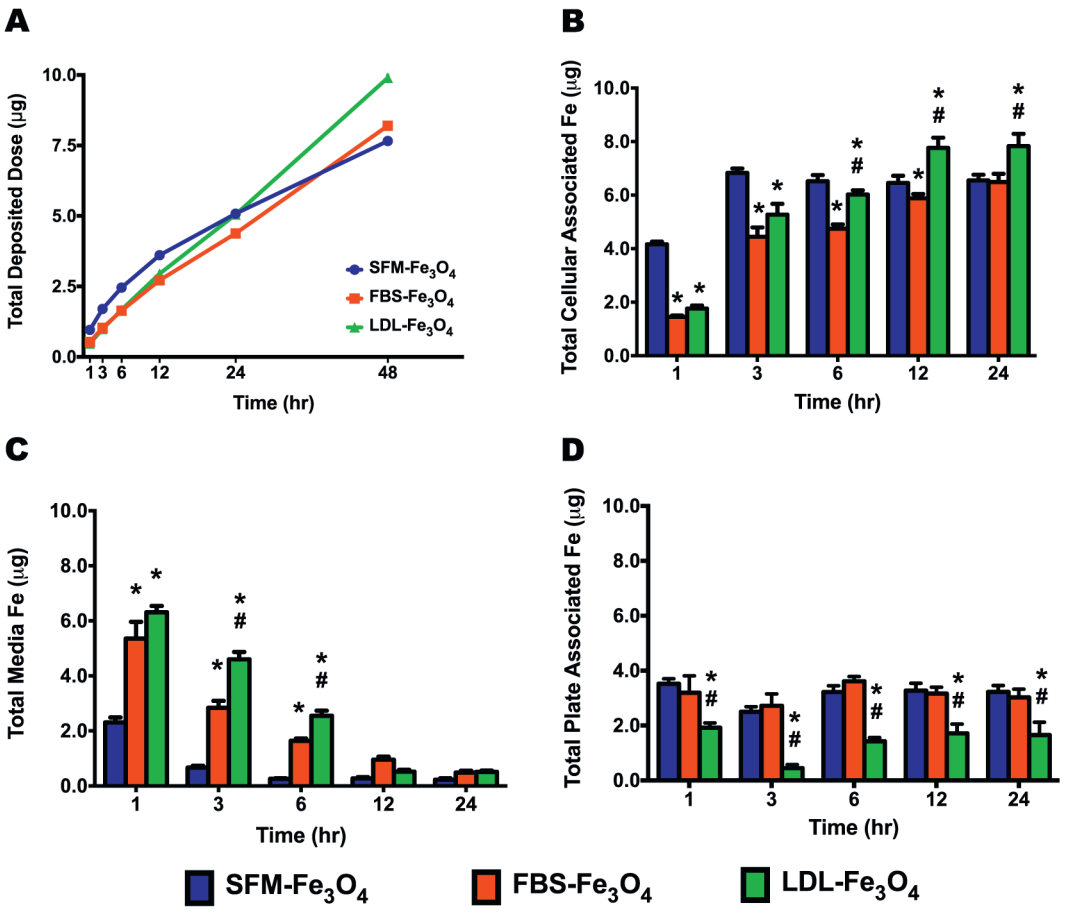

Fig. 1.

Deposition and cellular uptake of Fe_3O_4 NPs without or with BCs. (A) Representative deposition profile of Fe_3O_4 NPs without or with BCs based on *In Vitro* Sedimentation, Deposition, and Dosimetry (ISDD) Modeling over 48 h in a standard 24-well cell culture plate with 500 μL of media present (n = 6/group). (B) Total cellular associated Fe in macrophages cultured in standard 24-well plates with 500 μL of media present. (C) Total Fe remained in media. (D) Total plate associated Fe. Data represent mean + SEM, n = 6/group. *$p < 0.05$, as compared with the SFM-Fe_3O_4 NPs group; #$p < 0.05$, as compared with the FBS-Fe_3O_4 NPs group.

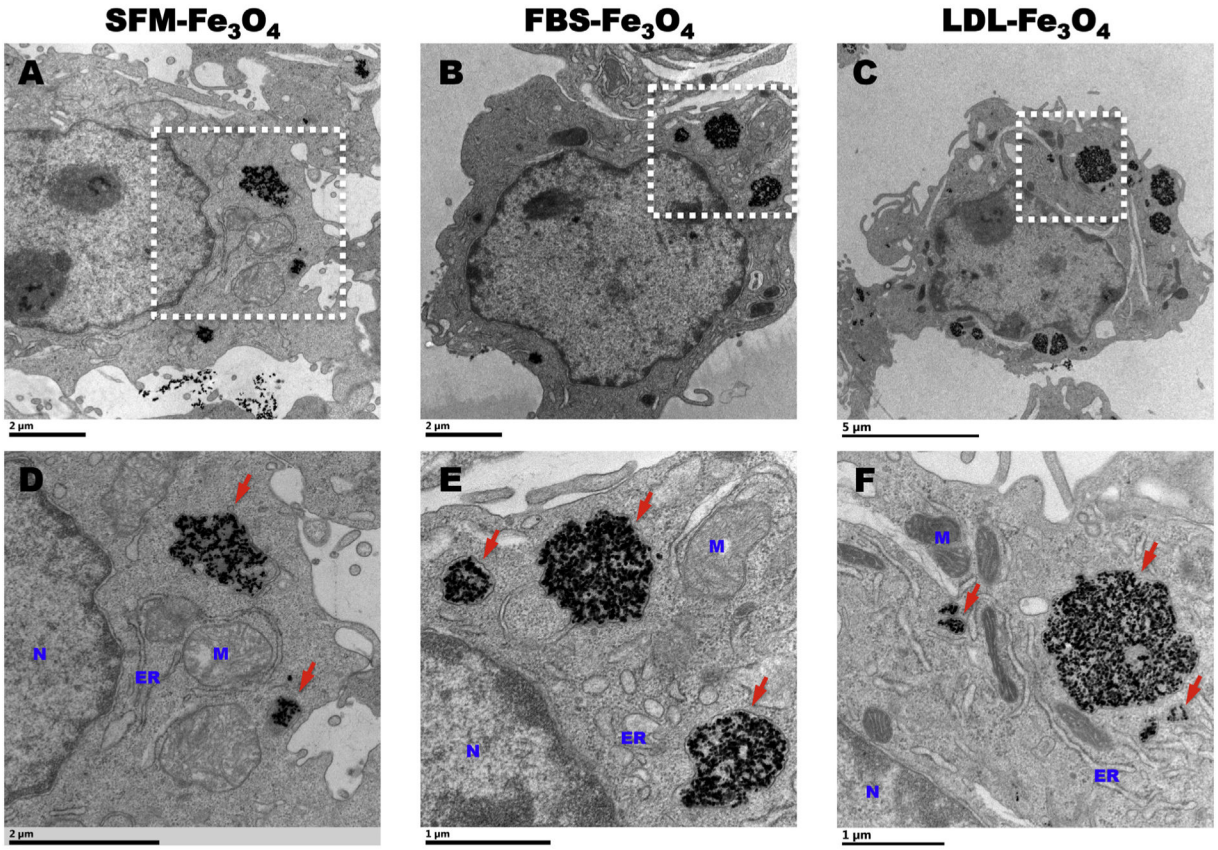

Fig. 2.

Internalization of Fe_3O_4 NPs in macrophages. (A), (B), and (C) are representative TEM images of internalized Fe_3O_4 NPs incubated in SFM, 10% FBS, 10% FBS + 200 mg/dL LDL in macrophages, respectively. Scale bar: 2 μm (A), 2 μm (B), and 5 μm (C). (D), (E), and (F) are representative high-resolution TEM images of internalized Fe_3O_4 NPs incubated in SFM, 10% FBS, 10% FBS + 200 mg/dL LDL in macrophages, respectively. N: nuclear; M: mitochondria; ER: endoplasmic reticulum. Red arrows point at the internalized Fe_3O_4 NPs as electron-dense NPs that are encapsulated by membrane as endosome-like vesicles. Scale bar: 2 μm (D), 1 μm (E), and 1 μm (F). (For interpretation of the references to colour in this figure legend, the reader is referred to the web version of this article.)

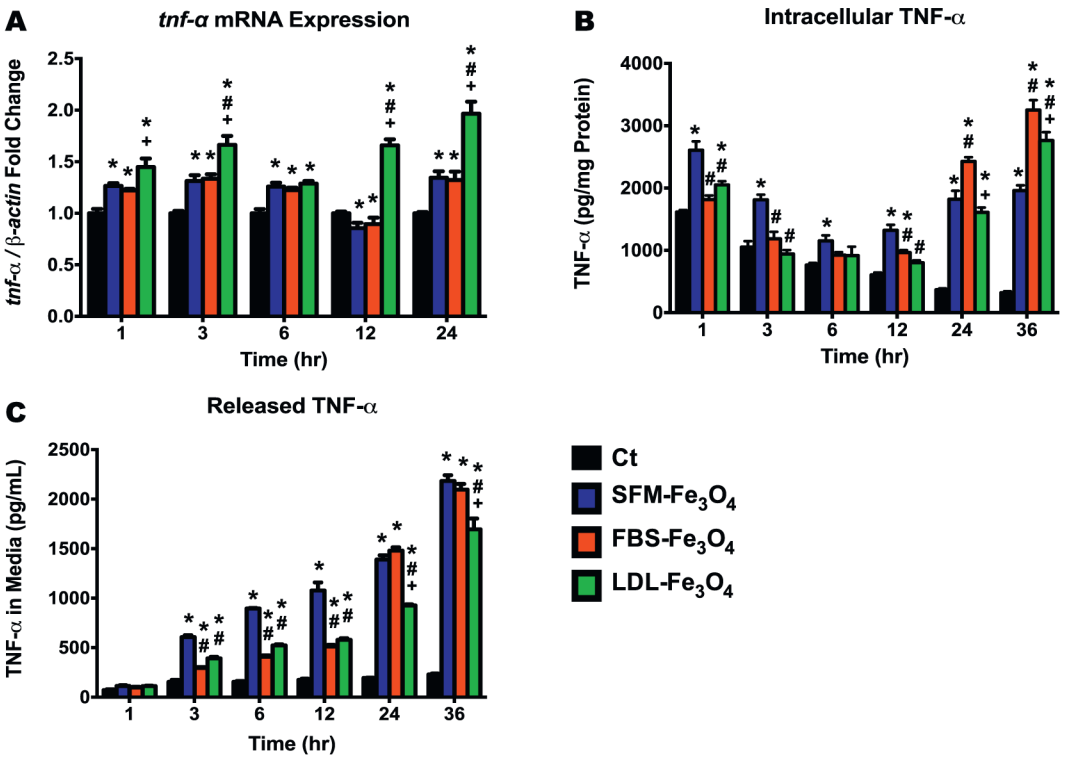

Fig. 3.

Transcriptional and protein expressions of TNF-α following exposure to Fe_3O_4 NPs without or with BCs. (A) *Tnf-α* mRNA expression (fold change compared to the control) in macrophages with or without NPs exposure. (B) Intracellular TNF-α levels (pg/mg protein) in macrophages with or without NPs exposure. (C) TNF-α levels (pg/mL) released in the culture media of macrophages with or without NPs exposure. Data represent mean + SEM, n = 6/group. *$p < 0.05$, as compared with the control group; #$p < 0.05$, as compared with the FBS-Fe_3O_4 NPs group; +$p < 0.05$, as compared with the FBS-Fe_3Q_4 NPs group.

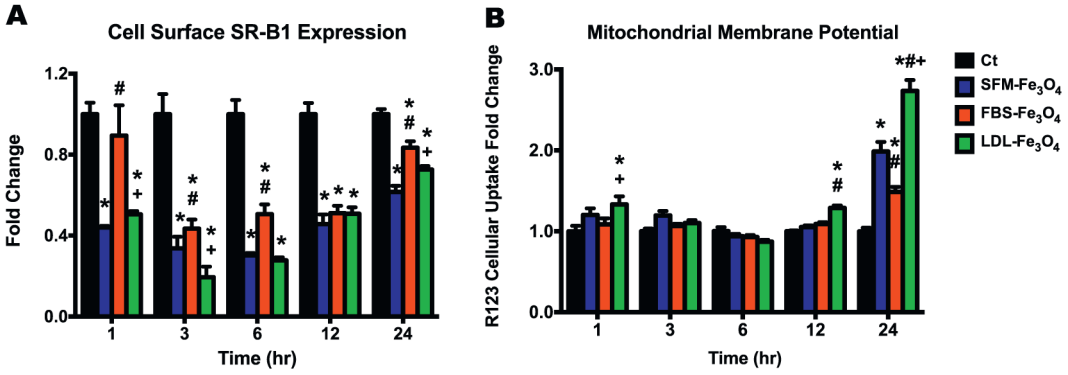

Fig. 4.

Cell surface expression of SR-B1 and MMP in macrophages with or without Fe_3O_4 NPs exposure. (A) Cell surface expression of SR-B1 (fold change compared to the control) in macrophages with or without Fe_3O_4 NPs exposure using fluorescent immunocytochemistry staining and flow cytometry analysis. (B) Intracellular Rhodamine 123 (R123) accumulation (fold change compared to the control) in macrophages with or without Fe_3O_4 NPs exposure. Data represent mean + SEM, n = 6/group. *$p < 0.05$, as compared with the control group; #$p < 0.05$, as compared with the SFM-Fe_3O_4 NPs group; +$p < 0.05$, as compared with the FBS-Fe_3O_4 NPs group.

Table 1

Fe_3O_4 NPs-Biocorona Characterization.

Nanoparticle - BC	Hydrodynamic size (nm)	Polydispersity index	Zeta potential (mV)
Fe_3O_4-H_2O	143.0 ± 2.4	0.26 ± 0.01	−41.13 ± 1.31
Fe_3O_4-SFM	76.1 ± 1.9 *	0.15 ± 0.01 *	−37.77 ± 0.85
Fe_3O_4-FBS	332.0 ± 9.3 *,#	0.28 ± 0.02 #	−34.53 ± 0.26 *
Fe_3O_4-FBS + LDL	525.6 ± 18.5 *,#,+	0.40 ± 0.02 #	−20.28 ± 1.05 *,#,+

Note: Data represent mean ± SEM, n = 9–12/group.

* $p < 0.05$, as compared with the Fe_3O_4-H_2O.

# $p < 0.05$, as compared with the Fe_3O_4-SFM.

+ $p < 0.05$, as compared with the Fe_3O_4-FBS.

Table 2

ISDD model-predicted time points that are needed to reach selected deposition fractions of the total administered dose.

% Deposited	SFM-Fe_3O_4 NP	FBS-Fe_3O_4 NP	LDL-Fe_3O_4 NP
25%	10h	15 h	14h
50%	33 h	35 h	29 h
75%	75 h	58 h	45 h
90%	131 h	83 h	60 h
95%	173h	99 h	69 h
99%	271 h	136 h	87 h
100%	> 480 h	480 h	215 h